Thermal Design of Power Electronic Devices and Modules

N. Delmonte*, M. Bernardoni, P. Cova and R. Menozzi
Dipartimento di Ingegneria dell'Informazione, University of Parma, Italy
*Corresponding author: viale G.P. Usberti 181/A, 43100 Parma, Italy, nicola.delmonte@unipr.it

Abstract: This work describes a way to apply 3D Finite Element (FE) analysis to the thermal design of power electronic modules using simplified geometry models of the system components. The method here presented can overcome the problem of solving equation systems with a very high number of Degrees Of Freedom (DOF) due to complex geometry of a power module.

Keywords: Thermal design, power devices, power modules, thermo-electromagnetic simulation.

1. Introduction

The experience made during teaching laboratory activities with COMSOL Multiphysics used to solve some thermal problems of power electronic devices, was helpful to setup the thermal design method of complex power module shown in following sections. The method proposed moves from the fact that usually in teaching activities we can't use computer with high computational capabilities. Then, to solve problems with complex geometries or high degree of freedom is necessary to design adequate simplified models of the real problems considered. The results obtained in the work presented here show that is possible to use simplified models of electronics power components to design FE model complex modules that lead to thermal results in good agreement with measurements.

The method is based on a detailed study of the individual components to be used in the modules. As will be shown, once the detailed model of a single component has been built, we develop a simplified model that satisfactorily approximates the thermal behavior of the detailed model. Then, we use these simplified component models in the thermal simulation of the whole system.

In this work we focus on the design of an high frequency DC/DC switching converter: the system features a few electromagnetic components, such as a primary inductor with toroidal core and secondary inductors with E cores, and MOSFET switches in SO8-bondless packages [1]. Fig.1 illustrates the modeling strategy for the whole power module.

The model was tuned by comparison with measurement performed on an ad-hoc designed FR4 test board operating at various output power levels. The model was then used to simulate the thermal behavior of an Insulated Metal Substrate (IMS) module, in order to evaluate the improvement in terms of maximum temperature and temperature gradients.

In the following paragraphs we will briefly show the modeling results for both the FR4 and the IMS boards.

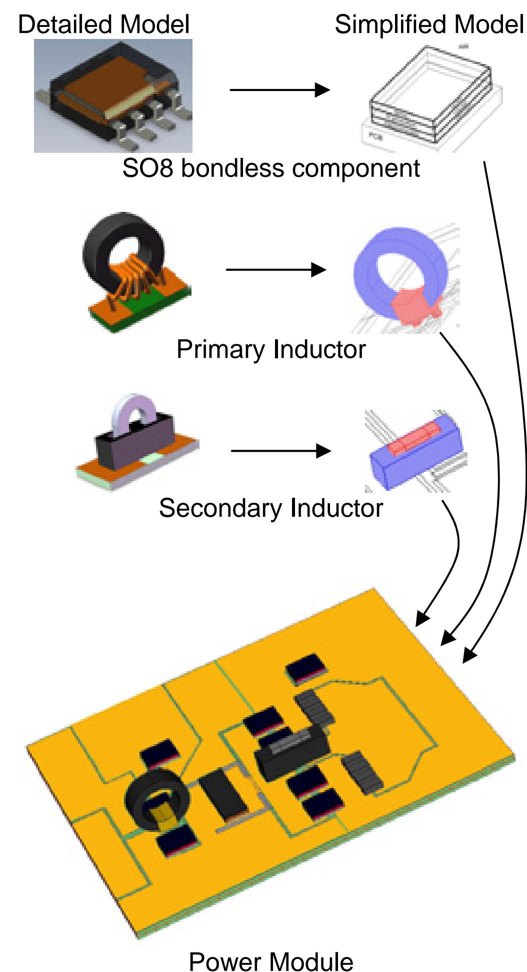

Figure 1. Electronic power module modeling workflow.

2. Numerical analysis with COMSOL Multiphysics

The converter used as test bench is a 1.8 MHz, 48 V half-bridge resonant voltage regulator [2]. It is made of two primary switches producing a square waveform, and a synchronous rectifier, connected by a resonant inductor, where the current flows with quasi-triangular shape, and a high-frequency transformer.

A prototype was built with a three-layer standard FR4 technology.

Numerical analysis was done using multi-physics 3D models.

2.1 Thermal model of active components

We designed a 3D FE thermal model of a single SMD transistor used in the half-bridge. We took as a reference structure that of the bondless SO-8 STS12NH3LL power MOSFETs, whose relevant characteristics were known, either from the literature or by optical (see Fig. 2(a)) and SEM (Scanning Electron Microscopy) inspection.

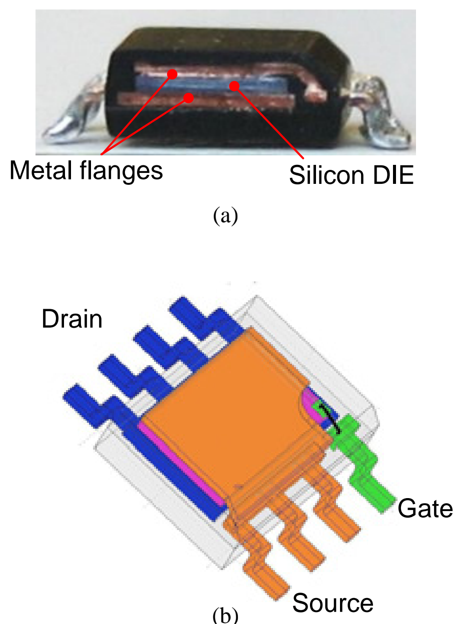

Figure 2. **(a)** Photograph of a sectioned SMD MOSFET; **(b)** 3D geometry of the STS12NH3LL power MOSFET: drain and source metallization are directly connected to the leads, without wire bonding.

The drain and source contacts are directly connected to the leads by metal flanges, while the gate contact is wire-bonded.

The COMSOL General Heat Transfer application mode has been used, which includes Fourier conduction and convection equations. The 3D geometry of the packaged transistor is shown in Fig. 2(b). The silicon die was modeled as the heat source and convective thermal boundary conditions were imposed at the external surfaces. In this model, unknown parameters were:

- the thermal resistance of the interface between the silicon die and the metal flange;
- the thermal conductivity of the package plastic lid;
- the thermal convection coefficient at the boundaries exposed to the air.

The values of these parameters were fixed by fitting experimental temperature data obtained from an *ad-hoc* designed test board shown in Figure 3, until we obtained a worst-case 10% error between simulated and measured temperature variations from ambient temperature on the test board.

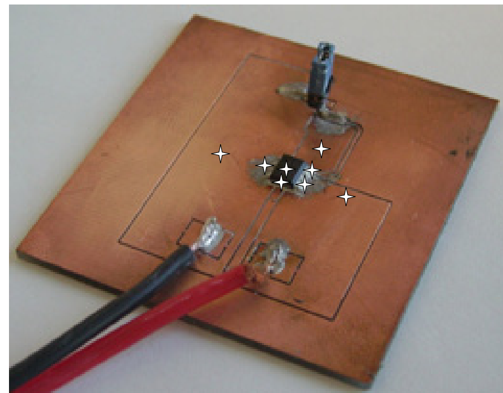

Figure 3. FR4 test board used for the simulation parameters tuning of the SMD MOSFET. The stars are centered on the test points.

To evaluate the external temperature of some points of the test board (see Fig. 3) the measurements were done using thermocouples, while the silicon die temperature were measured by an indirect method, using the drain to source voltage at a fixed drain current (I_D = 250 μA), as the temperature-sensitive parameter (TSP), because it has a large dependence on the channel temperature [3].

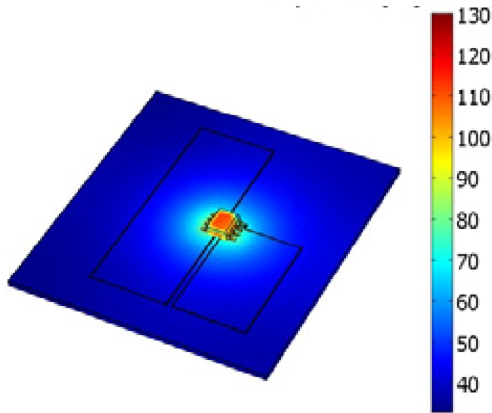

Figure 4. Boundaries temperatures [in °C] of FE MOSFET test board model. The MOSFET dissipates a power of 2.4 W.

For example, Fig. 4 shows the results of the simulations at the boundaries of the test board when the MOSFET dissipates 2.4 W.

After the accurate study of the STS12NH3LL, we developed a simplified model of the MOSFET and validated it by means of a comparison with the full model described above. The geometry of the simplified model shown in Fig. 5 consists in a three-layer parallelepiped with the same external surfaces as the real package; the leads are not simulated, and power is generated by an inner layer simulating the chip, in order to obtain the same temperature distribution as in the accurate model.

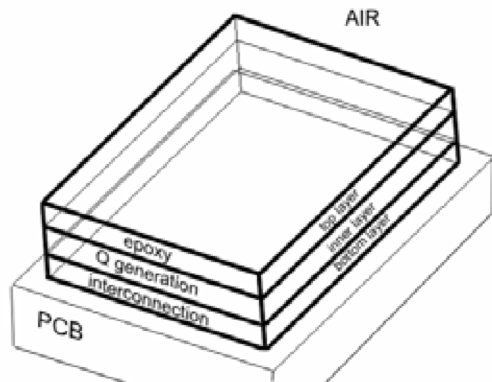

Figure 5. MOSFET simplified 3D geometry model.

2.2 Thermo-magnetic model of magnetic components

We developed an accurate thermal model of the two inductors embedded in the converter. The contributions of winding and core losses are separately modeled based on the results of electrical and electromagnetic simulations, respectively.

Since the converter works at 1.8 MHz, the skin depth is about 50 μm. The primary inductor is fabricated with a 7× Litz wire (see Fig. 6) with diameter of the individual internal wire of 200 μm: skin effect is therefore significant, and we took it into account as explained below. The secondary inductors practically work at constant current, so high frequency simulations are not required.

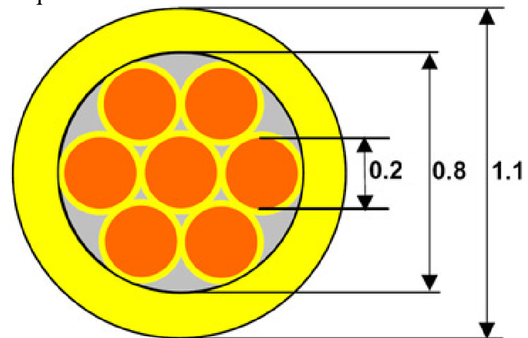

Figure 6. Schematic section of the Litz wire (dimensions in mm). Insulating layers are shown in yellow.

2.2.1 Primary inductor FE model

When building the 3D FE model of the primary resonant inductor, in order to keep the mesh complexity within manageable bounds, we did not simulate the Litz structure, but replaced it with a single solid wire and an *equivalent wire resistivity* as defined below. The copper area of the Litz wire is about 68% of the internal area (0.50 mm^2). The skin effect further reduces the effective area where the current flows. The length of the actual coil wire is about 100 mm, while the wire designed for the 3D FE inductor model has a diameter of 0.9 mm and a length of 85 mm.

We calculated the *equivalent wire resistivity* using the dissipated power density per unit length (0.17 W/m) extracted from a 2D simulation of a single internal wire of the Litz structure at the rated current I_{rms} = 4 A (Fig. 7), corresponding with an output current of 50 A, and at ambient temperature of 20°C; the total dissipated Joule power is therefore $0.17 \times 0.100 \times 7 = 0.12$ W: assuming this power to be uniformly dissipated on a single wire with a diameter of 0.9 mm and a length of 85 mm, we calculate the *equivalent electrical resistivity* to

be $5.6\cdot10^{-8}$ Ωm at 20°C (versus the actual copper resistivity of $1.7\cdot10^{-8}$ Ωm at 20°C). Similarly, the 3D complexity of the winding did not allow taking into account the external Litz wire cladding. In order to evaluate its impact on heat exchange, we performed a thermal simulation of a single linear Litz wire to evaluate the temperature difference between the external and internal surfaces of the insulator at I_{rms} = 4 A. The results are shown in Fig. 8. In order to perform the simulation under conditions similar to reality, the external cladding temperature was fixed at 100°C where the cladding is in contact with the toroidal magnetic core. The simulation shows a temperature difference well below 1°C.

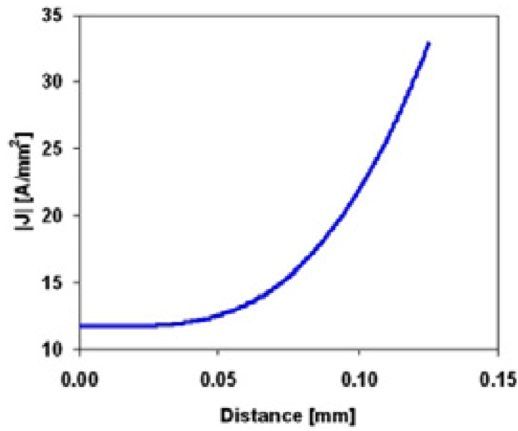

Figure 7. Simulated current density distribution [A/mm²] inside a single internal wire of the Litz structure at f = 1.8 MHz, I_{rms} = 4 A, T = 20°C. The distance on the x-axis is measured from the center along a radius.

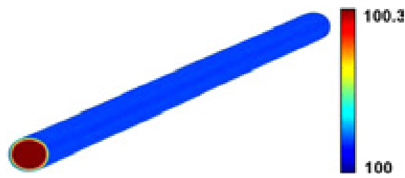

Figure 8. Temperature [°C] distribution in the insulated wire at I_{rms} = 4 A calculated with electro-thermal simulation.

With these simplifications, we built the 3D FE detailed model of the primary inductor, the geometry of which is shown in Fig. 1.

We then followed a three-step simulation method:

I. using the Conductive Media DC application mode, we simulated the Joule effect in the winding;

II. using the Quasi Static Electromagnetic application mode, we simulated the distribution of magnetic flux and eddy currents and the dissipated power density distribution in the core;

III. we input the dissipated power distributions calculated in the first two steps into the General Heat Transfer application mode to evaluate the temperature distribution.

The temperature dependences of the electrical conductivity of copper and of the core relative permeability are included in the model by the following expressions (T in K):

$$\sigma(T) = \frac{1}{5.6\cdot10^{-8}}\cdot\left[1-3.9\cdot10^{-3}(T-298)\right] \quad \text{(eq. 1)}$$

$$\mu(T) = 14\cdot\left[1-1.5\cdot10^{-4}(T-298)\right] \quad \text{(eq. 2)}$$

Magnetic losses for unit volume caused by 1.8 MHz current in the inductor core (Micrometal T50-14 Power Core) were included in the model by an empirical formula, supplied by the manufacturer, that relates the local flux density (B in Gauss) and frequency (f in Hz) with the local dissipated power density (p_s in mW/cm³):

$$p_s = \frac{f}{\frac{4\cdot10^9}{B^3}+\frac{3\cdot10^8}{B^{2.3}}+\frac{2.7\cdot10^6}{B^{1.65}}} + 1.6\cdot10^{-14} f^2 B^2 \quad \text{(eq. 3)}$$

As a thermal boundary condition, we fixed the temperature in proximity of the soldered wire ends at 71°C, as measured on the prototype converter under operating conditions (I_{rms} = 4 A, corresponding with converter output of V_{out} = 1.3 V, I_{out} = 50 A).

The temperature distribution at the boundaries of the model is shown in Fig. 9. The winding and inner core losses cause higher surface temperature in the bottom section of the core.

It is interesting to notice that the higher surface temperature of the bottom section of the core is not only due to the winding heat, but also to a larger flux density and therefore core loss, as shown in Fig. 10.

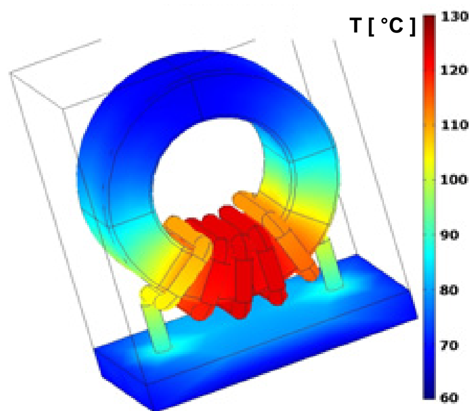

Figure 9. Simulated boundaries temperature distribution of the resonant inductor. I_{rms} = 4 A.

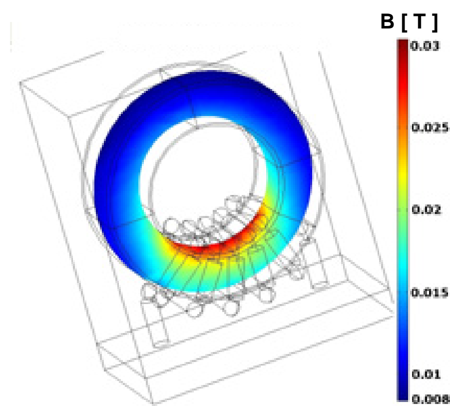

Figure 10. Simulated magnetic flux density in the central section of the resonant inductor core, under the same conditions as in Fig. 9.

The simplified model of the primary inductor that we designed to use in a complex power module FE model is shown in Fig. 1. This model has the same geometry as the more accurate model, save for the replacement of the wire by a compact strip, with the same volume, wrapped around the magnetic core. The strip is treated as a uniform power source, dissipating the same power as calculated by the detailed model.

2.2.2 Secondary inductor modeling

The secondary inductor was modeled by using the Conductive Media DC application mode, fully coupled with the General Heat Transfer application mode. In the Conductive Media DC mode, only the copper wire was activated imposing an inward current flow of 50 A. Obviously, because this inductor operates in DC mode, in the General Heat Transfer mode the only heat source is the wire. The geometry of the designed FE detailed model of this inductor is shown in Fig. 1.

In this case it was quite simple to simplify the model by modifying the wire geometry (see Fig. 1) and applying heat generation only in the sub-domain representing the wire.

2.3 Converter Thermal Model

Two different solutions have been studied for the power module: one using two layers of standard FR4 PCB (0.8 mm thickness) joined together to form a three-layer PCB with an equivalent total inner layer thickness of 0.14 mm, and the other built by depositing two resin layers (0.5 mm thickness) on both sides of a 0.7 mm thick copper baseplate. This kind of PCB is known as Insulated Metal Substrate (IMS). Fig. 11 shows the details of the two boards.

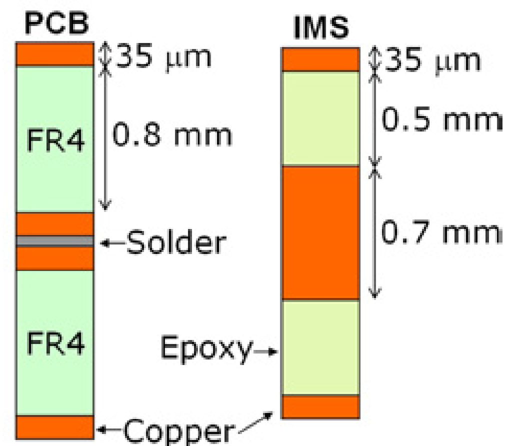

Figure 11. Layer structure of the two boards used for the converter prototypes.

The power components were mounted on both sides of the PCBs. Fig. 12 shows the converter prototype on the IMS board.

As mentioned above, from the accurate models of the MOSFET and inductors, we derived simplified models, suitable for the simulation of the full converter.

First, we considered the solution with standard FR4 PCB. In the FE model the heat exchange coefficients on the top and bottom sides of the board were adjusted to obtain the best fit between measured and simulated surface temperature distribution.

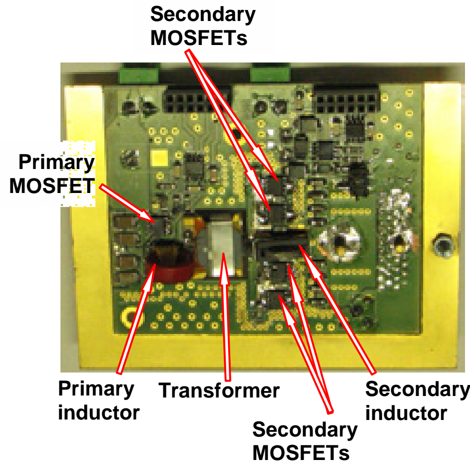

Figure 12. TOP view of the prototype with IMS PCB.

Accurate modeling of the planar transformer was not considered here. At the present stage, in the thermal simulations of the converter board, the planar transformer is replaced by a simplified 3-layer structure with a uniform heat source layer sandwiched between two insulating layers as done for the MOSFETs.

3. Results

A brief description of the results obtained for the module made with standard FR4 PCBs is given by Figures 13 and 14. Figure 13 shows the comparison between simulations and measurement results for two output current levels. As can be noticed, the agreement between the numerical models and the experimental data is good (the error in the temperature increase over ambient is below 10%).

Simulated (a) and measured (b) top surface temperature maps with 50 A load current can be seen in Fig. 14; measurements were performed using an IR camera at the Department of Information Engineering of University of Padova (Italy). Note that in Fig. 14-(b) there are some areas that at first glance seem to be at temperatures close to 30°C. This is due to uncalibrated measurement over metal surfaces with high radiation emissivity. To evaluate the temperature over some points of the boards, we black-painted the three areas shown in Figure 14-(b).

After fitting the model with standard FR4 PCBs, we applied the same fitting parameters to the model of the IMS solution.

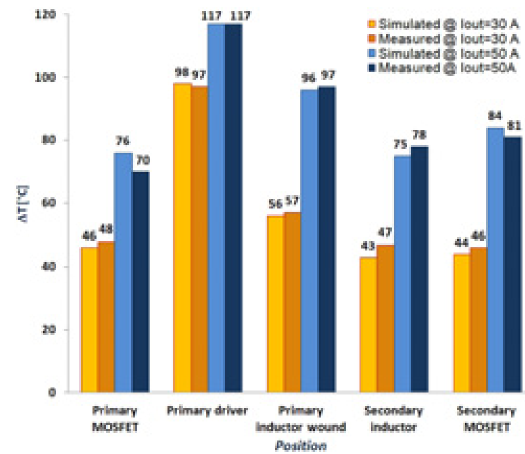

Figure 13. Measured and simulated temperature increase (over the ambient temperature of 26°C) at some points of the converter board (FR4 solution) for two load current levels.

We then compared the simulation results to measurements made on prototype with IMS board operating at different power levels.

For example, Table 1 shows the comparison between measured and simulated temperatures for the magnetic components in both solutions when the load current is 50 A.

The match between the measured and simulated temperatures of the IMS case is obviously worse, because the model was tuned for the standard FR4 PCB case and no further fitting was introduced for the IMS simulations.

However, the model captures the essential features of the temperature distribution over the whole board.

Component (test point)	ΔT [°C] (FR4)		ΔT [°C] (IMS)	
	Measured	Simulated	Measured	Simulated
Primary inductor wound	97	96 (-1%)	80	71 (-11%)
Primary inductor core	42	44 (+5%)	42	42 (<1%)
Transformer	95	99 (+4%)	82	73 (-11%)
Secondary inductor	78	75 (-4%)	70	61 (-13%)

Table 1. Measured and simulated temperature increase (over the 26°C ambient temperature) on the full converter board, for both the FR4 and IMS PCBs solutions, operating with a load current of 50 A.

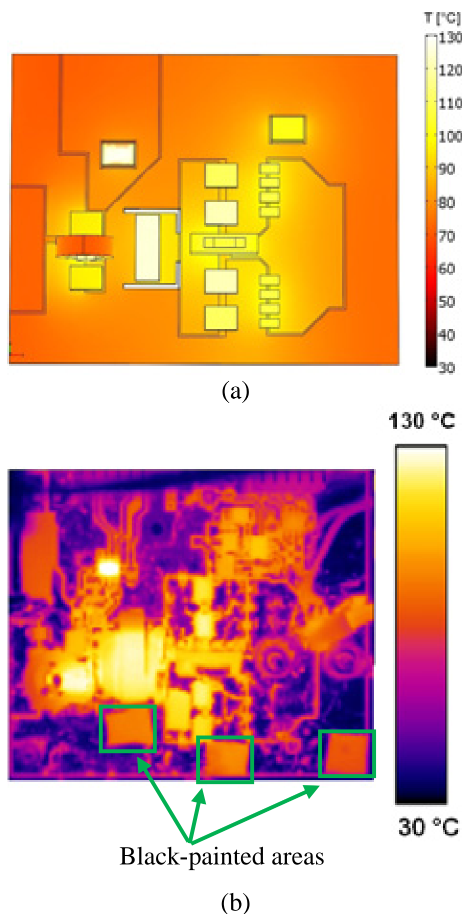

Figure 14. Thermal map of the top-side of the converter (FR4 solution) operating with 50 A load current: (a) simulated with COMSOL; (b) measured with IR camera.

The pictures of Fig. 15 can be used to compare simulation and measurement results of the IMS solution with the converter operating at a load current of 50 A.

4. Conclusions

This work focused on the thermal modeling of power converter boards. The inductors of a 1.8 MHz DC-DC switching converter are simulated using the Finite-Element (FE) approach with a three-step procedure: (i) electrical simulation for Joule power loss; (ii) electromagnetic simulation for core losses and eddy currents; (iii) thermal simulation for temperature distribution calculation.

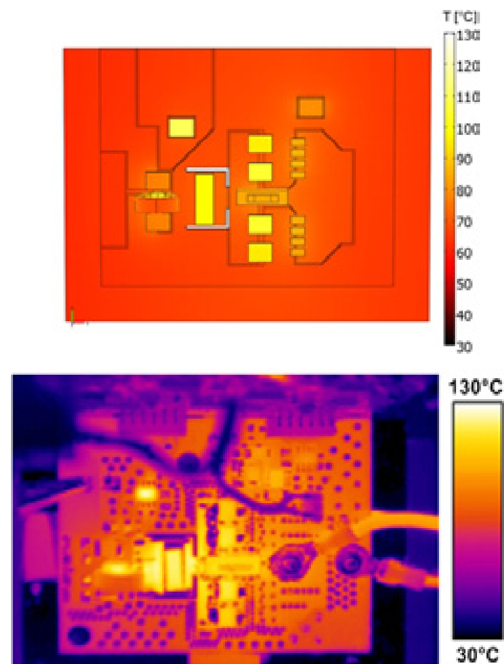

Figure 15. Thermal map of the up-side of the converter with IMS simulated (top) and measured with the IR camera (bottom) with 50 A load current.

The accurate FE model is used as reference to build simplified models that can be used in the FE thermal simulation of the whole converter board.

The results we obtained are encouraging, and indicate that this approach can be a valuable tool providing designers with a way to evaluate the interaction between electrical, magnetic and thermal effects while choosing the proper components, materials and layout for the converter.

5. References

1. "STS25NH3LL *data sheet"*, ST microelectronics (2003)

2. L. Huber, K. Hsu, M. Jovanovic, 1.8 MHz, 48 V resonant VRM, *IEEE Trans. on Power Electronics*, **Volume 1, n. 1**, pp. 79-88 (2006)

3. B.J. Baliga, *Modern Power Devices*, pp. 327-329. John Wiley & Sons, New York (1987)

4. *AC-DC Module User's Guide* - COMSOL version 3.4, (2007)

5. *Heat Transfer Module User's Guide* - COMSOL version 3.4. (2007)